On predicting the sound from a cavitating marine propeller in a tunnel

Antti Hynninen,[1] **Jukka Tanttari,**[1] **Ville M. Viitanen,**[1] **Tuomas Sipilä**[1]

[1]VTT Technical Research Centre of Finland Ltd., Espoo, Finland

ABSTRACT

Model tests in a cavitation tunnel are commonly used in order to predict the radiated noise from full-scale marine propellers. Correction factors and scaling procedures are commonly used in estimating the effects of background noise and the propeller model scale. Less attention is paid to the influence of the tunnel related factors. Above a certain frequency, i.e. first non-plane wave mode cut-on frequency, the sound pressure varies over the tunnel cross-section and non-plane waves are introduced. Below this frequency, only plane waves propagate in the tunnel and no attenuation due to geometrical spreading occurs in the far field of the propeller. Thus, it is difficult to apply source level scaling procedures based on, e.g., spherical spreading of the sound field. Also, rigid tunnel walls near the propeller load it acoustically and may alter the fundamental sound emission compared to emission of the same source in free field conditions. In this paper, sound emission and immission of acoustic sources in a free space and in a waveguide are discussed and sound from a cavitating model-size marine propeller in a tunnel is investigated with numerical methods.

Keywords

cavitation, marine propeller noise, acoustic analogy, hybrid method

1. INTRODUCTION

Marine propeller represents one of the most important sources of underwater radiated noise. The generated sound due to blade loading and turbulence has a continuous broadband spectrum with tonal peaks at the blade passing frequency and its harmonics. Above the cavitation inception speed the sound generation is dominated in the low frequency tones due the fluctuations of the cavitation volumes as the propeller blades move through the non-uniform flow. Collapse of global cavitation structure leads to broadband sound when the propeller blades pass through the non-uniform flow created by the wake of hull surfaces and appendages located forward of the propeller.

Common way to estimate the radiated noise from full-scale marine propellers is to conduct the model test in a cavitation tunnel. A compendium of tunnel- and hydrophone installations is available in Bark and van Berlekom (1979); Doolan et al. (2013); Felli (2011); Jeona and Joob (2014); Tani et al. (2016). The diversity of installations in use is large. This may cause problems when results between different premises are compared or transferred to other conditions. The guidelines given by the International Towing Tank Conference ITTC (2014) are fairly loose.

In addition to clarifying the phenomena of sound emission and immission of acoustic sources in a free space and in a waveguide, sound from a cavitating model-size marine propeller in a tunnel is investigated with numerical methods. In the propeller noise simulations, a two-step hybrid approach is used. Cavitation and the turbulent flow around the propeller are calculated with computational fluid dynamics (CFD) and the acoustic fields are computed with finite element method (FEM)-based acoustic analogies. The accuracy of the sound sources computed with Unsteady Reynolds Averaged Navier Stokes (URANS)-based CFD is improved by using conformal surfaces in the vicinity of the propeller in acoustic FEM. With this hybrid approach, the interactions of boundary surfaces i.e. tunnel walls is implicitly taken into account.

2. SOUND EMISSION AND IMMISSION

The categories of acoustic measurements are emission, transmission and immission (Lang et al., 2006). Sound energy is emitted by the source, transmitted to a receiver, where it is "immitted".

Immission is usually quantified as sound pressure level at certain location. It depends on transfer path, i.e., acoustic environment and the positions of source and receiver.

Emission (total output) of a source is described using two quantities, sound power (in Watts) and directivity. Directivity is a measure of variation of sound radiation with direction, often stated as a function of angular position.

In certain conditions, sound pressure can be used to quantify emission. The conditions are (i) free field in the source far

field and (ii) diffuse reverberant field in a special reverberation chamber. The free field method uses the relation of measured sound pressure p and sound intensity I [Watts/m^2] of a propagating plane wave. Sound intensity is integrated over a surface S enclosing the source and scaled to sound power W. Surface normal component of intensity I_n in the free far field at distance r from the source is

$$I_n(r) \approx \frac{p(r)^2}{\rho_0 c_0}, \tag{1}$$

where spherical spreading $p \sim 1/r$ of the wave front is assumed, when using equation (1) at different distances in free space. Sound power W_S determined at the surface is

$$W_s = \int_S I_n dS. \tag{2}$$

In equations (1) and (2), ρ_0 is fluid density, c_0 is speed of sound and S is the surface of sound power evaluation. Note that equation (1) does not apply, unless the receiver points are in the free far field of the source. In the far field, the source-receiver distance is large compared both to the wavelength of sound and to the size of the source. This is also the basic idea of determination of ship source level: sound pressure measurement in the free far field followed by the normalization of result to 1 meter distance from the assumed source point, e.g. ANSI/ASA (2009). Intensity-pressure relation of equation (1) without spherical spreading applies also to a propagating plane wave in a duct or a tunnel.

2.1. ITTC guidelines for model scale noise measurements

Acoustic signatures of model scale propellers are measured in cavitation tunnels. ITTC (2014) gives guidelines to that. The document states that "noise measurements are usually performed in order to predict the full scale acoustic source strength of the cavitating propeller". At least implicitly source strength means sound emission.

The main operations in the ITTC guidelines are (i) distance normalization, (ii) correction for reflections from tunnel walls, (iii) correction for background noise and (iv) scaling to full scale size. The points (i) and (ii) are of interest here.

In the distance normalization, sound pressure measured at distance d from the source is transformed to a reference distance d_{ref} = 1 m. According to the guidelines, spherical spreading is usually assumed. Because the source is not a point source, cylindrical spreading might be another possibility for a first approximation (Viitanen et al., 2017).

About corrections for reflections from tunnel walls ITTC (2014) guideline states: "In order to assess the influence of these reflections, an acoustic calibration could be made using a known sound source put at specific locations in the test section. A transfer function between source and the received acoustic signal of the measurement system is then obtained provided that the coherence between the received signal and the source signal is close to one." This description leaves the exact correction procedure open.

A simple correction procedure for wall reflections using the "known source" could be carried out as follows. The source is placed in specified positions in the cavitation tunnel (subscript CT). Level $L_{p,CT}$ is measured. The free-field (subscript FF) sound pressure level $L_{p,FF}$ using the same source and receiver position(s) is measured as well. The difference is the correction term $L_{p,trans}$

$$L_{p,trans} = L_{p,FF} - L_{p,CT}. \tag{3}$$

The correction term is assumed to apply for the propeller source (subscript $prop$) measured in the tunnel, and corrected to the free field

$$L_{p,FF,prop} = L_{p,CT,prop} + L_{p,trans}. \tag{4}$$

There are obvious problems in the ITTC procedure. The first is that no spherical (or cylindrical) spreading occurs in the tunnel environment.

The second problem is that the correction measured for a certain type of source does not apply to another, maybe very different type of source.

The third, an implicit, problem is that measurements in the source near field should be avoided. The reasons to this are that (i) the near-field of a real source is extremely complicated and hence location sensitive and (ii) the near field may be dominated by the reactive part of sound field. Reactive part is not propagating to the far field but rather sloshing back and forth.

2.2. Measurement method modelling using BEM

A boundary element method (BEM) model was used to simulate acoustic fields in a 12 meters long, water-filled tunnel, Figure 1. The tunnel sidewalls are rigid and perfectly reflecting. The ends are reflection-free. The tunnel cross-section is 600 x 600 mm. The speed of sound is 1554.6 m/s and the density of water is 999.7 kg/m^3. Models were solved from 20 to 3000 Hz with 20 Hz resolution.

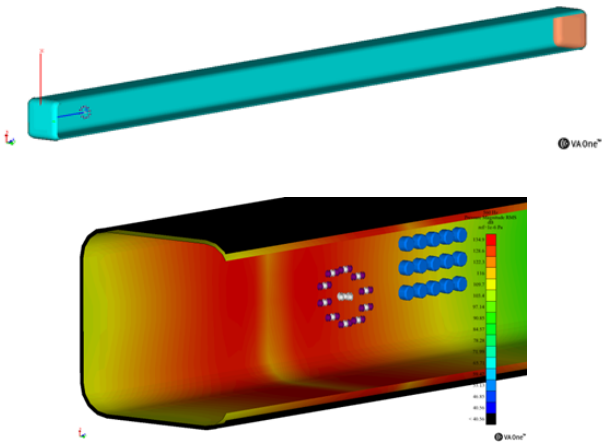

Figure 1: BEM model of the tunnel. Top: overall view; Bottom: source end with 20 monopoles active and some point sensors (blue dots).

A source array is located at 1 meter distance from the other end. The array consists of 39 simple (monopole with a given volume velocity) sources. By modifying the source strengths and their phases, many different types of source arrays can be used to drive the acoustic field inside the tunnel. In this paper we used (i) individual monopoles and (ii) a ring of 10 phased dipoles (20 monopoles) forming a rotating source ("dipole ring") of diameter 187.5 mm. The center of the ring is at the center of the cross section and the dipoles are oriented along the tunnel longitudinal axis.

The main purpose of the model was to study sound fields induced by different source types and use the results to assess different kind of measurement strategies. Sound pressure at any point as well as sound power of any source combination can be easily calculated. A free field BEM model (Figure 2) was also created for calculation of the correction term of equations (3) and (4).

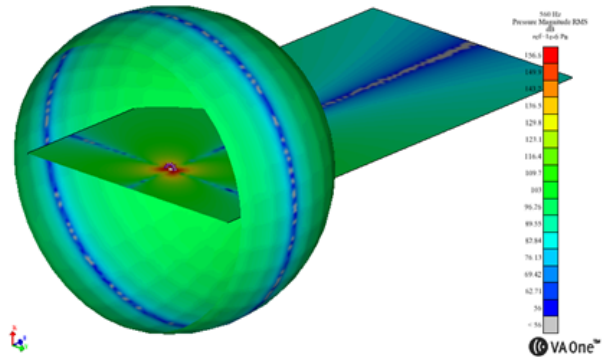

Figure 2: The free-field BEM model with planar and spherical data recovery surfaces.

It is possible to include the elasticity, and hence vibration and sound radiation of the walls, into the model. This interesting topic is beyond the scope of this paper.

3. ACOUSTIC SOURCE IN A FREE SPACE AND IN A WAVEGUIDE

In free space far field conditions, acoustic waves spread radially from the source. The distribution of sound pressure at certain distance but different angles depends on the directivity. However, the local wave front approaches asymptotically a plane wave and spreading of sound pressure in certain direction follows the $1/r$-law.

Conditions in a tunnel are completely different. The propagation is limited to the axial direction by the tunnel walls. Up to high frequencies, tunnel walls are at the near field of the source. The walls load the source acoustically and change its behavior.

3.1. Waveguide modes in a rectangular tunnel

In a tunnel, only certain types of waves, called waveguide modes propagate. Each mode has a characteristic pressure interference pattern at the tunnel cross section and a cut-on frequency, above which the mode can propagate. Calculated mode patterns and cut-on frequencies for a 600 x 600 mm square cross-section are shown in Figure 3.

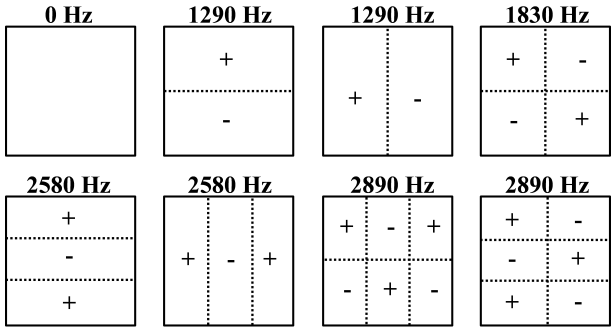

Figure 3: Waveguide mode patterns and their cut-on frequencies in a 600 x 600 mm tunnel. Speed of sound is 1554.6 m/s. The dashed lines are nodal lines, where sound pressure of the mode is zero.

The lowest mode is called the plane wave mode. It has a constant pressure distribution on the cross section and it propagates at all frequencies. As the frequency increases, more complicated modes can propagate, see e.g. Fahy (2000). In the plane wave mode, a plane wave propagates purely axially.

The higher order modes are composed of an interfering set of oblique plane waves reflected from the walls. The total field is a combination of the waveguide modes. It depends on frequency and the distribution of sources.

3.2. Characteristics of sound field in a waveguide

Figure 4 shows the difference in fields generated at 1500 Hz, when a monopole source is located at the center or at the corner of the cross section. The propagating modes are excited differently because of different source location.

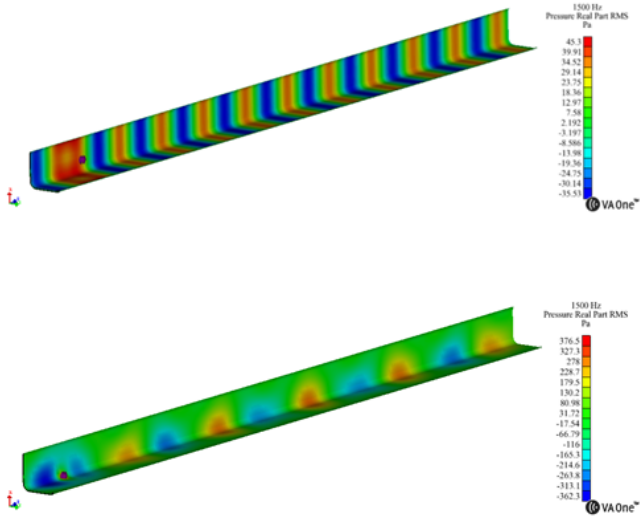

Figure 4: Tunnel wall instantaneous sound pressure in Pa at 1500 Hz. Top: source is a monopole at the center, exciting the plane wave mode; Bottom: monopole source at the corner of the cross section, exciting the higher order modes as well.

When a waveguide mode is excited below its cut-on frequency, there is practically no propagation to the far field, nor net power input. However, there a very rapidly decaying evanescent near field in the vicinity of the source, see Figure 5. In this case the source does not excite the plane wave mode.

Figure 5: Evanescent near field at 500 Hz for a dipole ring source.

3.3. Sound pressure sensitivity for the source distance

Sound pressure level at different distances along the tunnel axis for a center monopole and the dipole ring are shown in Figure 6. Below the cut-on frequency of the first higher order mode there is a huge difference between the sources in behavior of the sound pressure. Evidently, it is not meaningful to transform induced sound pressure of either of the sources from 2 to 0.5 m using the spherical spreading assumption, i.e., adding 12 dB to the levels.

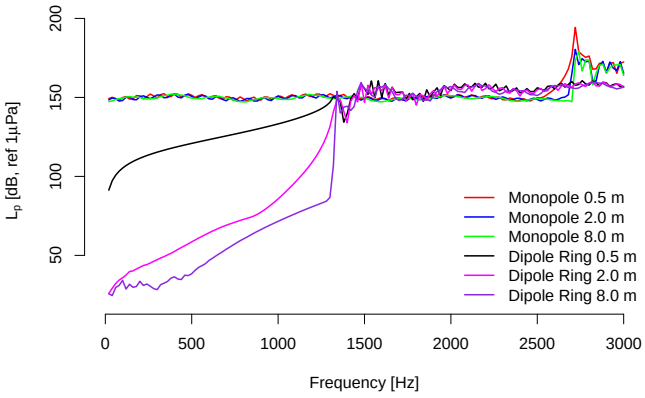

Figure 6: Sound pressure sensitivity for the axial distance from the source. Sound pressure levels for a center monopole and a dipole ring averaged over the cross section at distances of 0.5, 2 and 8 m from the source plane.

3.4. Sound pressure sensitivity of the receiver location

Single-point sound pressure can be very sensitive to the location of the point, i.e. receiver location. 17 sensors were placed in two lines forming a cross-like array at the wall of the tunnel, Figure 7. Center of the array is 0.2 meters from the source plane. Sensors cover a length 0.5 meters in both directions.

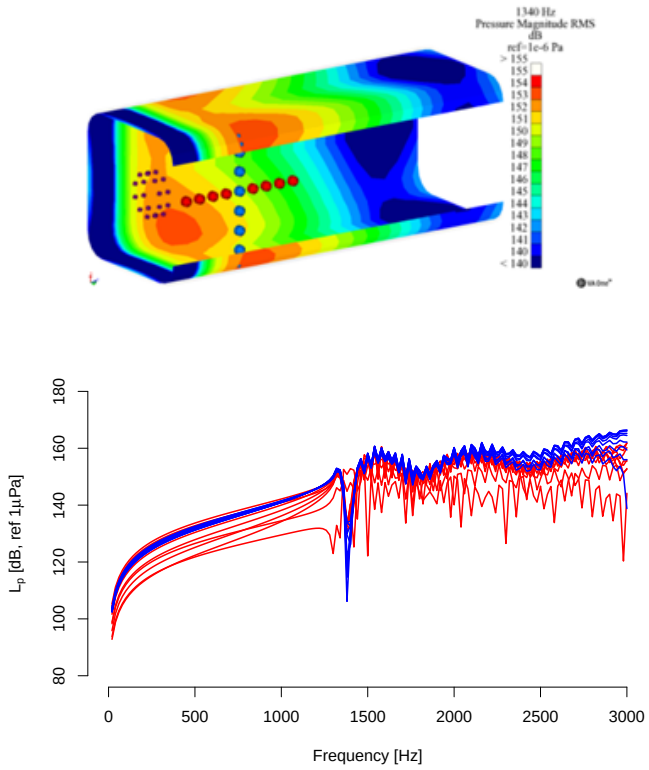

Figure 7: Sound pressure sensitivity of the receiver location at the tunnel wall for a dipole ring source. Top: 17 sensors placed on vertical and axial lines at a tunnel wall; Bottom: induced sound pressure levels, blue curves: vertical line sensors, red curves: axial line sensors.

The results scatter up to 30 dB. At low frequencies below 1300 Hz, the scatter is stronger in the axial direction. It is caused by the rapid decay of the evanescent near-field (see Figure 5). There is practically no scatter in vertical direction at low frequencies. At higher frequencies, higher order modes start to produce also more scatter in the vertical direction. Since the source is composed of longitudinally oriented dipoles, the level is lowest at the source plane. One of the axial line sensors is located at that plane. That particular sensor has the lowest levels although it is located closest to the source.

3.5. Correction for sound pressure at a single receiver point

According to equation (3), a correction term is needed to transform the result from the tunnel to the free space. An example of calculated corrections for five individual point pairs at distances is shown in Figure 8. In these results, the mutual positions of the source and receiver are the same in the tunnel and in the free space. However, all the corrections are different. Even in the case of very simple source the correction is not universal, but depends on the exact positions of the source and receiver in the tunnel. More complicated sources typically produce more scattered results.

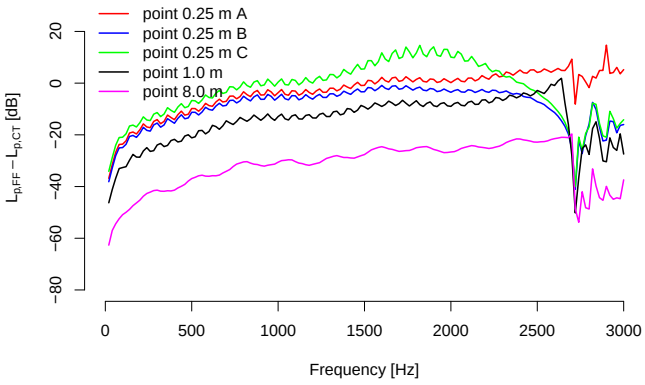

Figure 8: The correction terms for sound pressure level induced by a single monopole at individual point pairs. Response points are located roughly 0.25 (three different points), 1.0 and 8.0 meters from the source.

3.6. Correction for sound power

Sound power quantifies the total acoustic output and it is not tied to any point or distance. It is known, see e.g. Pierce (1989), that the radiated power from an acoustic monopole in free field is

$$L_{W,FF} = \frac{2\pi|\hat{S}|^2}{\rho_0 c_0}, \tag{5}$$

where $|\hat{S}|$ is the monopole amplitude. The radiated power from a point source in a duct, e.g. cavitation tunnel, is

$$L_{W,CT} = \frac{4\pi^2|\hat{S}|^2 c_0}{A\omega^2\rho_0}, \tag{6}$$

where A is the cross-sectional area of the duct. Note that equation (6) is valid only in the plane wave frequency range. Correction term $L_{W,FF}$-$L_{W,CT}$ defined for sound power overcomes the problem associated with corrections based on single points. The correction terms for sound power levels for a single monopole placed at the center, at the corner of the tunnel cross-section and for a dipole ring are shown in Figure 9.

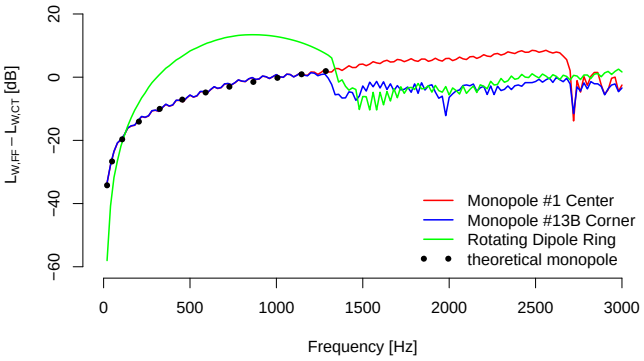

Figure 9: The correction terms for sound power levels for a single monopole placed at the center, at the corner of the tunnel cross-section and for a dipole ring. Theoretical curve for a monopole is from Pierce (1989).

The correction still depends on source itself and its position and orientation in the tunnel. At low frequencies the monopole results fit to the theoretical correction for a monopole presented by Pierce (1989). At high frequencies there are more and more propagating modes and the correction tends asymptotically to 0 dB.

4. PROPELLER NOISE SIMULATIONS

In this study, underwater noise generation and propagation are assumed to be decoupled, i.e. flow-generated noise does not impact the internal dynamics of the flow. Therefore, hybrid method is justified. Hydroacoustic sources are computed from the unsteady hydrodynamics solved with CFD. The hydroacoustic sources are transformed from the time domain to the frequency domain and the propagation of the acoustic waves is solved in frequency domain using acoustic FEM.

4.1. Propeller in a cavitation tunnel

A propeller from SVA Potsdam was selected as a test case (Barkmann et al., 2011). The open Potsdam Propeller Test Case (PPTC) data is intended to offer the possibility to test and validate calculation method(s). In this report, the propeller in uniform homogeneous inflow condition is studied numerically in cavitating condition. The propeller is operating in push configuration. Here, propeller in the operation point one is investigated. That is the advance coefficient J=1.019 and the cavitation number σ_n=2.024. This corresponds to the PPTC Case 2.3.1 of smp'11 Workshop (Barkmann et al., 2011).

Acoustic underwater noise simulation model was built with Hypermesh software. CAD model of the PPTC in a cavitation tunnel depicted in Figure 10 was received from SVA Potsdam.

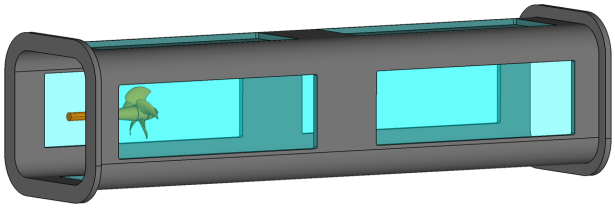

Figure 10: CAD model of the PPTC propeller in the cavitation tunnel.

Conformal surfaces around the propeller blades and propeller hub are created for the acoustic source data extraction from CFD results and for the creation of the Lighthill's surface sources to the acoustic mesh. The conformal surfaces used in this study are presented in Figure 11.

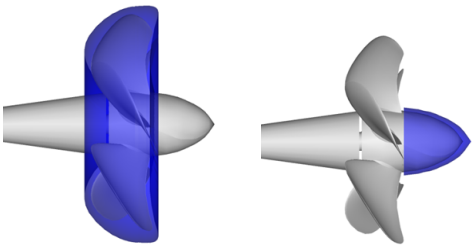

Figure 11: Conformal surfaces for the source data generation. Left: conformal surface for the propeller blades; Right: conformal surface for the propeller hub.

Finest CFD grid is used as the starting point for the acoustic source determination, i.e. 5.5 million cells per blade with $k-\varepsilon$ turbulence model. See Viitanen et al. (2017) for details on the experiments and CFD simulations.

Acoustic FEM mesh is created for the fluid, i.e. tunnel volume minus the volume enclosed by the conformal surfaces and the propeller shaft assembly. Acoustic FEM mesh of the fluid is shown in Figure 12. The mesh consists of approximately 500 000 elements, i.e. more than six elements per wavelength up to 3600 Hz. Ends of the cavitation tunnel are modelled as non-reflecting boundaries. Acoustic contributions from the conformal surfaces for the propeller blades and for the propeller hub as well as the conformal volume for the wake field are studied separately. The conformal surfaces and the

conformal volume downstream in the vicinity of the propeller are shown in Figure 12.

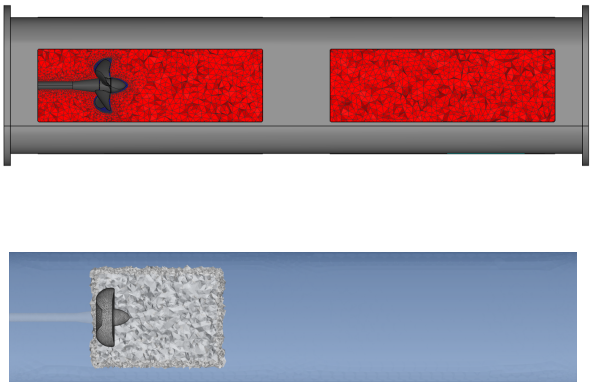

Figure 12: Top: acoustic FEM model of the cavitation tunnel fluid; Bottom: conformal surfaces for the propeller blades and for the propeller hub as well as the conformal volume of the wake field.

4.2. Lighthill's analogy

The solution to the acoustic problem is based on the acoustic analogy. In acoustic analogies, flow equations are re-arranged so that on the left side there is acoustic wave equation and what is left on the right side is the "source". The different noise generation mechanisms are expressed using separate source terms. Analogies are derived from basic formulas of gas dynamics, conservation of mass and conservation of momentum equations. See Uosukainen (2011) for the foundations and details of analogies. In this study, the Lighthill's analogy is used (Lighthill, 1952, 1954). In Lightill's analogy, density is the acoustic primary variable. Using the formulation as in ACTRAN software (Actran, 2016), the original Lighthill's analogy wave equation in the frequency domain is

$$\frac{\omega^2}{c^2}\psi + \frac{\partial^2 \psi}{\partial x_i \partial x_j} = \frac{1}{i\omega}\frac{\partial^2 \tilde{T}_{ij}}{\partial x_i \partial x_j}, \tag{7}$$

where transformed potential

$$\tilde{\rho} = -\frac{i\omega\psi}{c^2} \tag{8}$$

is used, c is the speed of sound and $\tilde{\rho}$ is the density. Lighthill's tensor is approximated by

$$\tilde{T}_{ij} \approx \tilde{\rho}\tilde{v}_i\tilde{v}_j. \tag{9}$$

The weak variational formulation of the equation in Actran FEM contex is

$$\begin{aligned} -\int_\Omega \frac{\omega^2}{\rho_0 c^2}\psi\delta\psi d\Omega - \int_\Omega \frac{1}{\rho_0}\frac{\partial\psi}{\partial x_i}\frac{\partial\delta\psi}{\partial x_i}d\Omega = \\ \int_\Omega \frac{1}{\rho_0\omega}\frac{\partial\delta\psi}{\partial x_i}\frac{\partial T_{ij}}{\partial x_j}d\Omega - \int_\Gamma \frac{1}{\rho_0}\mathcal{F}(\tilde{\rho}\tilde{v}_i n_i)d\Gamma \end{aligned} \tag{10}$$

The RHS of equation (10) consists of a volume source term and a surface source term. In this study, the contributions of these terms are studied separately. That is, the contribution from the propeller blades, propeller hub, and from the wake field are evaluated.

The source terms are calculated in time domain using oversampling by default at every half CFD time steps to avoid aliasing effects during the Fourier transform, and saved in an NFF database. The calculated hydroacoustic source terms are then transformed on the acoustic mesh by integrating over the CFD mesh using the shape functions of the acoustic mesh.

4.3. Propeller acoustic source contributions

The mean sound pressure level in the cavitation tunnel for propeller blades, hub and wake field are shown in Figure 13. The source contributions at 100 Hz are depicted in Figure 14. In the figures, the acoustic pressure maps, corresponding iso-surfaces and pressure maps at the cut plane are shown.

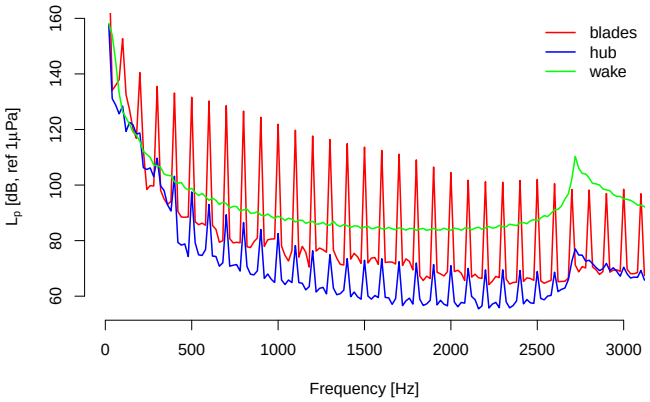

Figure 13: Mean sound pressure level in the cavitation tunnel for propeller blades, hub and wake field.

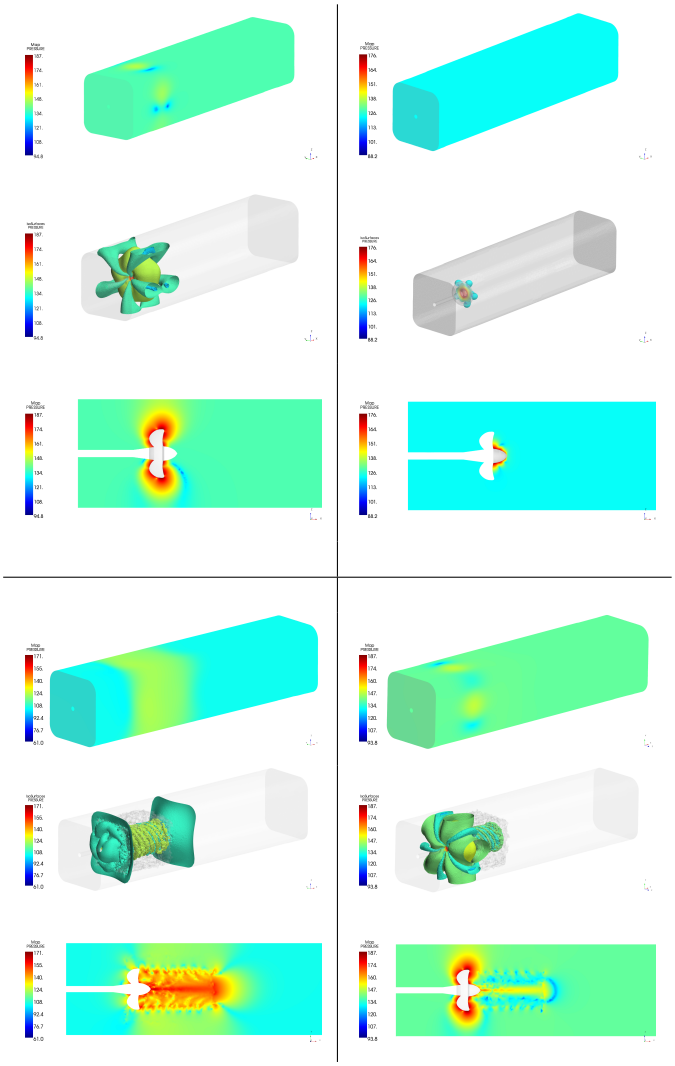

Figure 14: Top left: acoustic source contribution at 100 Hz from the propeller blades; Top right: from the propeller hub; Bottom left: from the propeller wake field; Bottom right: total acoustic contribution.

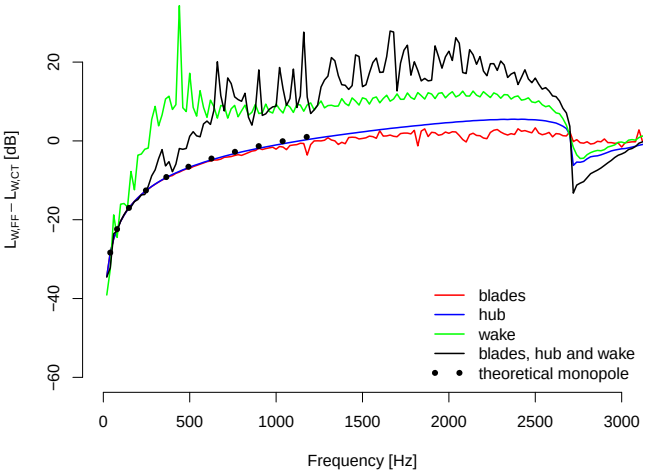

Figure 15: Correction for sound power level for propeller blades, hub and wake field. Also the total correction and the theoretical correction for an acoustic monopole are drawn.

4.4. Propeller source type estimation

In order to have an insight to the acoustic source type of the propeller, the acoustic free field FEM model of the propeller was also investigated. By comparing the acoustic powers of the propeller computed in the free field and in the cavitation tunnel the correction $L_{W,FF} - L_{W,CT}$ for the sound power is derived. The corrections for the propeller blades, propeller hub and for the propeller wake field are shown in Figure 15. In the figure, also the total correction and the theoretical correction for the acoustic monopole according to Pierce (1989) are shown.

5. DISCUSSION AND CONCLUSIONS

In this paper, it was shown that the characteristics of a sound field in a wave guide is highly dependent on the source and its position and orientation. The excitation and decay of waveguide mode patterns shown in Figure 3 are frequency dependent. Even for a known source, the sound pressure level is very sensitive to the axial distance from the source as shown in Figure 6. In can be noted from Figure 7 that measuring the source at the near field should be avoided. A correction term is needed to transform the result from the tunnel to the free space. Even in the case of a very simple source, the correction depends on the exact positions of the source and receiver as shown in Figure 8. Correction for sound power overcomes the problem associated with the corrections based on single points. Unfortunately, the sound power correction still depends on the source and its position and orientation in the tunnel, see Figure 9.

In the propeller noise simulations, a two-step hybrid approach was used. It is clearly visible in Figure 13, that the cavitating propeller blades have the strongest impact on the sound pressure level at the blade passing frequency and its harmonics. The wake field acts as an acoustic source in wide frequency range. The peak at approximately 2700 Hz is due the excitation of the unsymmetrical tunnel mode. In Figure 14 it is also notable that the sound pressure at the tunnel walls is very different than the sound pressure in the vicinity of the propeller

and in the wake field. The sound pressure distribution seems reasonable.

Corrections for the sound power level for PPTC were derived taking separately into account the contributions from the propeller blades, propeller hub and the wake field. It can be noted from Figure 15 that the correction for propeller hub is equal with the theoretical monopole. Also the cavitating propeller blades seem to act like a monopole source. Due to the wake field contribution, the total correction for the sound power level differs greatly from the monopole type.

Sound emission of ducted fans is routinely characterized using sound power. Measurements are done by integrating sound pressure over the duct cross-section at a measurement station several duct diameters downstream from the fan. Duct terminations are reflection free. Procedures are described in an international standard (ISO, 2003).

As a final conclusion, it can be noted that the sound emission of a cavitating marine propeller in a tunnel should be characterized using sound power. Then, the numerical methods should be verified with measurements.

Question from Thomas Lloyd

Why do you use Lighthill acoustic analogy instead of for example Ffowcs Williams-Hawkings analogy? Which sources are included? The difference in directivity of the wake source could be due to it being a quadrupole source i.e. Lighthill stress tensor. Do you agree?

Author's closure

The most general approach to fluid acoustics consists in solving the compressible Navier-Stokes equations through a direct numerical simulation (DNS). The solution includes sound generation and propagation. Unfortunately DNS is numerically very expensive. One alternative approach is to use acoustic analogies, as first proposed by Lighthill (Lighthill, 1952, 1954).

In the acoustic analogies, the noise generation and propagation are assumed to be decoupled, that is, flow-generated noise does not impact the internal dynamics of the flow. In the acoustic analogies, the equations governing the acoustic field are rearranged in such a way that the field variable connections are on the left-hand side and the source quantities on the right hand-side. Lighthill's analogy, Powell's analogy, Ffowcs Williams-Hawkings analogy and Curle's analogy are density-based analogies, i.e. they use perturbation of density or acoustic pressure as the basic field quantity. See Uosukainen (2011) for the foundations and details of analogies.

The Ffowcs Williams-Hawkings analogy is based on the same starting point and assumptions and equations as Lighthill's analogy, but it takes also into account the effects of moving boundaries and additionally, it is possible to take into account the influence of rigid semi-infinite baffles.

The key is to use the variational formulation of Lighthill's analogy in finite element method (FEM) context as done in this paper. With this procedure the moving boundaries are naturally taken into account and there are no limitations on the elasticity or geometry of the surrounding boundaries (Actran, 2016). Therefore this procedure is suitable also for full scale underwater hydro-vibro-acoustic simulations of cavitating marine propellers.

We agree that the wake creates quadrupole type sources. However, the acoustic FEM procedure used in this paper does not distinguish the different source types. Importance of the different source typers must be studied in detail in the future.

Question from Zhihui Liu

Why use the conformal surface as the acoustic source surface but not the propeller surface?

Author's closure

It is convenient to use rotationally symmetric acoustic source surface which totally encloses the rotating propeller. With this procedure the acoustic source surface is time-invariant. Finding the best possible conformal surface needs further studies.

References

Actran, MSC. (2016). 'User's guide release 16'. Free Field Technologies.

ANSI/ASA. (2009). 'Quantities and Procedures for Description and Measurements of Underwater Sound from Ships – Part 1: General Requirements', American National Standard, American National Standards Institute, New York, USA.

Bark, G. & van Berlekom, W. B. (1979). 'Experimental investigations of cavitation dynamics and cavitation noise'. Twelfth Symposium of naval hydrodynamics, National Academy of Sciences, Washington DC, pp. 470-493.

Barkmann, U., Heinke, H.-J., & Lübke, L. (2011). 'Potsdam propeller test case (PPTC)'. Proceedings of the Second International Symposium on Marine Propulsors smp'11,

Hamburg, Germany. Workshop: Propeller performance, pp. 36–38.

Doolan, C., Brandner, P., Butler, D., Pearce, B., Moreau, D. & Brooks, L. (2013). 'Hydroacoustic characterisation of the amc cavitation tunnel'. Proceedings of Acoustics 2013, Victor Harbor, Australia.

Fahy, F. J. (2000). Foundations of engineering acoustics. Academic press.

Felli, M. (2011). 'Noise measurements techniques and hydrodynamic aspects related to cavitation noise'. HydroTesting Alliance (HTA), Sustainable Surface Transport. Project No.: 031316, Sixth Framework Programme Priority 1.6.2.

ISO5136. (2003). 'Acoustics - Determination of sound power radiated into a duct by fans and other air-moving devices - In-duct method', International Standard, International Organization for Standardization, Geneva, Switzerland.

ITTC. (2014). 'ITTC - Recommended Procedures and Guidelines, Model scale noise measurements'. 27th International Towing Tank Conference ITTC, Copenhagen, Denmark. Specialist Committee on Hydrodynamic Noise, Section 7.5-02-01-05.

Jeona, J.-H. & Joob, W.-H. P. (2014). 'Prediction of propeller radiated noise by onboard measurement'. UA2014 2nd Underwater Acoustics Conference and Exhibition, Rhodes, Greece. pp. 667–674.

Lang, W. W., Maling, G. C., Nobile, M. A. & Tichy, J. (2006). 'Determination of sound power levels and directivity of noise sources'. Noise and Vibration Control Engineering: Principles and Applications, ed. Beranek, L. L. & Ver, I. L., 2nd ed. John Wiley & Sons Inc., pp. 71–118.

Lighthill, M. J. (1952). 'On sound generated aerodynamically. I. general theory'. Proceedings of the Royal Society of London A: Mathematical, Physical and Engineering Sciences, **211**, pp. 564–587.

Lighthill, M. J. (1954). 'On sound generated aerodynamically. II. turbulence as a source of sound'. Proceedings of the Royal Society of London A: Mathematical, Physical and Engineering Sciences, **222**, pp. 1–32.

Pierce, A. D. (1989). Acoustics: An Introduction to its Physical Principles and Applications. Acoustical Society of America, New York.

Tani, G., Viviani, M., Hallander, J., Johansson, T. & Rizzuto, E. (2016). 'Propeller underwater radiated noise: A comparison between model scale measurements in two different facilities and full scale measurements'. Applied Ocean Research, **56**, pp. 48–66.

Uosukainen, S. (2011). Foundations of Acoustic Analogies. VTT Technical Research Centre of Finland, Espoo. VTT publications 757.

Viitanen, V. M., Hynninen, A., Tanttari, J., Sipilä, T., Lübke, L., Klose, R. & Siikonen, T. (2017). 'CFD and CHA simulation of the underwater noise induced by a marine propeller in two-phase flows'. Proceedings of the Fifth International Symposium on Marine Propulsors smp'17, Espoo, Finland.